COBEM 2021 26th International Congress of Mechanical Engineering
November 22-26, 2021, Virtual Congress, Brazil
ABCM Associação Brasileira de Engenharia e Ciências Mecânicas

COB-2021-1365
Boundary conditions effects on the boiling heat transfer problem in channels using the lattice Boltzmann method

Luiz Eduardo Czelusniak
Alfredo Jaramillo Palma
Luben Cabezas-Gómez
Department of Mechanical Engineering, Heat Transfer Research Group, São Carlos School of Engineering (EESC), University of São Paulo (USP), São Carlos 13566-590, Brazil
Alexander J. Wagner
Department of Physics, North Dakota State University, Fargo, North Dakota 58108, USA
luiz.czelusniak@usp.br, ajaramillopalma@gmail.com, lubencg@sc.usp.br, alexander.wagner@ndsu.edu

Abstract. *Processes involving phase change in liquid-vapor mixtures inside channels are of great interest in mechanical engineering due to the advantages that this phenomenon provides in refrigeration systems in terms of heat transfer efficiency. Systems of this type are found in different applications such as domestic refrigeration, nuclear reactors and electronics cooling. There is a high scientific interest in the development of numerical tools capable of simulating this type of systems. A promising tool in this regard is the lattice Boltzmann method (LBM). One LBM extension to simulate multiphase flows is the pseudopotential method which consists in the addition of a fluid-fluid interaction force. This additional term naturally induces and allows coexistence of different fluid phases. In this work, the pseudopotential LBM is applied to the study of boiling heat transfer in channel flows. The Multi-relaxation time (MRT) collision operator will be used in the lattice Boltzmann equation in order to increase simulation stability. The Peng-Robinson equation of state (EOS) will be used and its parameters will be selected in order to approximate the fluid behavior to that of water. The LBM is employed along a suitable energy conservation equation. Also, bubble nucleation is induced by applying temperature perturbations at the walls. In this work, two discrete outflow boundary conditions (convective and Neumann null conditions) are tested and their impact on stability and bubble nucleation is assessed. This work will contribute to a better understanding about current strengths and limitations of the pseudopotential method in the simulation of boiling in channel flows. From these results, improvements of the method may be devised in order to improve its accuracy.*

Keywords: *Outflow Boundary Conditions, Boiling Heat transfer, Channel Flow, Lattice Boltzmann Method.*

1. INTRODUCTION

The mathematical modeling of boiling heat transfer is a challenging problem that has many industrial applications, such as cooling of nuclear reactors, computer chips and other electronic devices (Park *et al.*, 2016; Genk, 2012; Pulvirenti *et al.*, 2010). The physical phenomena involved in this problem are quite complex, with non-linearities arising from the two-phase nature of the flux. The Lattice Boltmann equation (LBE), which corresponds to a discrete version of the Boltzmann transport equation, is a numerical tool that has received great deal of attention during the last two decades (Krüger *et al.*, 2017; Sukop and Thorne, 2006), as it is a suitable framework for handling mesoscale physics.

Several numerical and experimental works have demonstrated the capability of LBM simulations to incorporate two-phase features like surface tension and contact angle, at different Reynolds regimes and different boundary conditions for the mass and heat fluxes. Zhang and Chen (2003) proposed a *hybrid* methodology to simulate boiling heat transfer based on a pseudopotential field: while the mass flux is modeled by mean of a LBM, the heat flux is computed employing a classical Finite Difference Method. Their method recovered thermodynamic consistency and it was shown to be robust. The incorporation of a tunable surface tension along a pseudopotential was studied by Li and Luo (2013), augmenting the capabitily of the LBM as previous works did not considered pressure variations across the phases interface. Also, this hybrid method have recently been used in pool boiling simulations with heat transfer (Guzella *et al.*, 2020).

Regarding the contact angle, several models based on the pseudopotential approach were reviewed by Li *et al.* (2014). The authors proposed a modified model and gave recommendations on what type of model to use depending on the contact angle's magnitude. Recently, in a work by Hu *et al.* (2016) the authors stressed that this type of method can introduce an artificial diffuse interface between the bulk phase fluid and the solid walls and proposed a *geometric method* that does not suffer from that issue.

Studies considering microchannels require the imposition of inflow/outflow conditions, for which numerical results when considering heat flux are scarse. An example of such study was made by Jafari and Okutucu-Özyurt (2016) by means

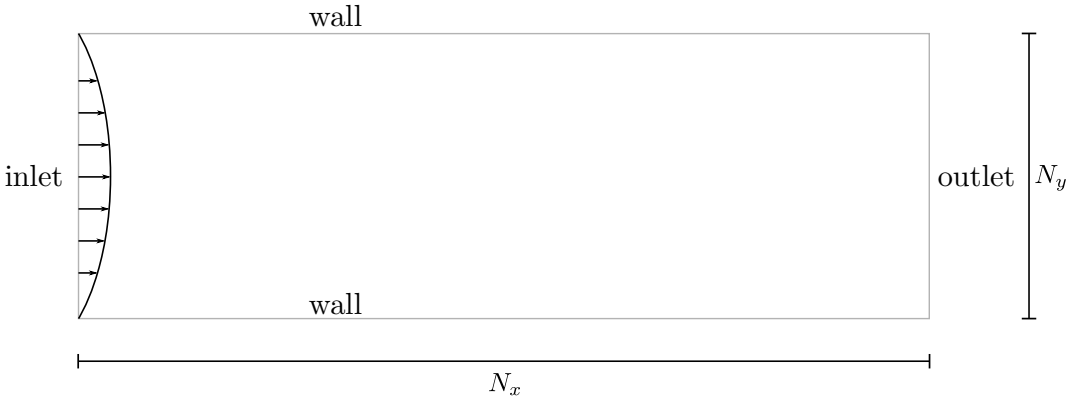

Figure 1. Scheme of the physical configuration.

of a Finite Element Method along the Cahn-Hillard phase-field method. However, that kind of *continuum* methodology suffers from having to impose *a priori* nucleation sites, which represents an issue when studying bubbles nucleation, and it can be tackled by means of the LBM (Li *et al.*, 2020).

In this work, we adapt different methods to impose inflow/outflow conditions found in the literature for LBM simulations (Sohankar *et al.*, 1998; Lou *et al.*, 2013), first stability results are reported when varying the Reynolds number and the dependence of bubble nucleation on these methods is assessed.

2. MATHEMATICAL MODELING

A scheme of the channel's configuration is shown in Figure 1, a parabolic velocities profile developed along the horizontal axis is prescribed at the left boundary and outflow conditions are set at the right boundary.

2.1 Hydrodynamic model

The velocities space is discretized along the D2Q9 set, given by

$$\mathbf{c}_i = \begin{cases} (0,0), & i = 0, \\ (1,0),(0,1),(-1,0),(0,-1), & i = 1,\dots,4, \\ (1,1),(-1,1),(-1,-1),(1,-1), & i = 5,\dots,8. \end{cases} \tag{1}$$

Denoting by $\mathbf{x}$ and t the space and time coordinates, resp., for each of these velocities one associates a distribution function $f_i(\mathbf{x},t)$ that gives the number of particles at time t positioned between $\mathbf{x}$ and $\mathbf{x}+d\mathbf{x}$ that have the velocity $\mathbf{c}_i$, and which evolution is governed by the LBE

$$f_i(\mathbf{x}+\Delta t\,\mathbf{c}_i, t+\Delta t) - f_i(\mathbf{x},t) = \Omega_i(\mathbf{f},\mathbf{f}^{\text{eq}})(\mathbf{x},t), \tag{2}$$

where $\mathbf{f}$ is the vector of components $[\mathbf{f}]_i = f_i$ and $\Omega_i(\mathbf{f},\mathbf{f}^{\text{eq}})$ is the collision operator. The multirelaxation time (MRT) collision operator (Krüger *et al.*, 2017) is employed to improve stability, and it can be written as (adding upon the repeated index)

$$\Omega_i(\mathbf{f},\mathbf{f}^{\text{eq}}) = -\left[\mathbf{M}^{-1}\mathbf{\Lambda}\mathbf{M}\right]_{ij}(f_j - f_j^{\text{eq}}) \tag{3}$$

where $\mathbf{\Lambda}$ is the relaxation matrix and $\mathbf{M}$ is the matrix converting f into the momentum space, chosen as

$$\mathbf{M} = \begin{pmatrix} 1 & 1 & 1 & 1 & 1 & 1 & 1 & 1 & 1 \\ -4 & -1 & -1 & -1 & -1 & 2 & 2 & 2 & 2 \\ 4 & -2 & -2 & -2 & -2 & 1 & 1 & 1 & 1 \\ 0 & 1 & 0 & -1 & 0 & 1 & -1 & -1 & 1 \\ 0 & -2 & 0 & 2 & 0 & 1 & -1 & -1 & 1 \\ 0 & 0 & 1 & 0 & -1 & 1 & 1 & -1 & -1 \\ 0 & 0 & -2 & 0 & 2 & 1 & 1 & -1 & -1 \\ 0 & 1 & -1 & 1 & -1 & 0 & 0 & 0 & 0 \\ 0 & 0 & 0 & 0 & 0 & 1 & -1 & 1 & -1 \end{pmatrix}$$

and the relaxation matrix is set to

$$\mathbf{\Lambda} = \text{diag}\left(\tau_\rho^{-1}, \tau_e^{-1}, \tau_\zeta^{-1}, \tau_j^{-1}, \tau_q^{-1}, \tau_j^{-1}, \tau_q^{-1}, \tau_\nu^{-1}, \tau_\nu^{-1}\right).$$

The computations related to (3) are simplified thanks to the relations (Krüger *et al.*, 2017)

$$\mathbf{m}^{\text{eq}} \equiv \mathbf{M}\mathbf{f}^{\text{eq}} = \left(\rho,\ -2\rho + 3\rho|\mathbf{u}|^2,\ \rho - 3\rho|\mathbf{u}|^2,\ \rho u_x,\ -\rho u_x,\ \rho u_y,\ -\rho u_y,\ \rho(u_x^2 - u_y^2),\ \rho u_x u_y\right)^{\intercal},$$

and thus (2) and (3) are separated into the collision step

$$\begin{cases} m_i \leftarrow \mathbf{M} f_i \\ m_i^* \leftarrow m_i - \mathbf{\Lambda}(m_i - m_i^{\text{eq}}) + \Delta t\, S_i \\ f_i^* \leftarrow \mathbf{M}^{-1} m_i^* \end{cases}, \tag{4}$$

where the additional terms S_i correspond to momentum sources, and the streaming step

$$\left\{\ f_i(\mathbf{x} + \mathbf{c}_i \Delta t, t + \Delta t) \leftarrow f_i^*(\mathbf{x}, t)\right. \quad , \tag{5}$$

Let us recall that ρ and $\mathbf{u}$ can be computed in terms of the first and second moments of the distributions $\mathbf{f}$

$$\rho = \sum_i f_i, \qquad \rho\mathbf{u} = \sum_i f_i \mathbf{c}_i + \frac{\mathbf{F}}{2},$$

where $\mathbf{F} = (F_x, F_y)$ corresponds to the force field and $\mathbf{u} = (u_x, u_y)$ to the velocities field. This force field includes intermolecular forces (used to account for the two-phase behavior of the fluid) according to the Shan and Chen model (Chen and Doolen, 1998)

$$F_\alpha^{\text{SC}}(\mathbf{x}, t) = -G\,\psi(\mathbf{x}, t) \sum_i w_i \psi(\mathbf{x} + \Delta t\,\mathbf{c}_i, t)\, c_{i\alpha}, \tag{6}$$

where ψ is the pseudopotential field and G is a tunable numerical parameter set to -1 in this work. The pseudopotential is related to an equation of state (EOS) according to

$$\psi(\mathbf{x}, t) = \sqrt{\frac{2(p_{\text{EOS}}(\mathbf{x}, t) - \rho(\mathbf{x}, t)/3)}{G}}\,, \tag{7}$$

with p_{EOS} given be the Peng-Robinson EOS

$$p_{\text{EOS}} = \frac{\rho R T}{1 - b\rho} - \frac{a\rho^2 \left[1 + \left(0.37464 + 1.54226\,\omega - 0.2699\,\omega^2\right)\left(1 - \sqrt{T/T_c}\right)\right]^2}{1 + 2b\rho - b^2\rho^2}.$$

where $T = T(\mathbf{x}, t)$ is the temperature field, T_c is the critical temperature, ω is the acentric factor, R is the universal gas constant, $a = 0.45724\, R^2 T_c^2 / p_c$, $b = 0.0778\, R T_c / p_c$, and p_c is the pressure at the critical point. In this work, these parameters have been set to $T_c = 0.1094$, $\omega = 0.344$, $a = 3/49$, $b = 2/21$ and $R = 1$ in lattice units.

2.2 Thermal model

The Partial Differential Equation for the temperature field reads (neglecting viscous work, Li *et al.* (2020))

$$\rho\, c_{\text{V}} \left(\partial_t T + \mathbf{u} \cdot \nabla T\right) = \nabla \cdot (\lambda \nabla T) - T \left(\frac{\partial p_{\text{EOS}}}{\partial T}\right)_\rho \nabla \cdot \mathbf{u}\,, \tag{8}$$

with c_{V} being the specific heat at constant volume, $\lambda(\mathbf{x}, t) = c_{\text{V}}\, \alpha(\mathbf{x}, t)\, \rho(\mathbf{x}, t)$ the thermal conductivity. The thermal diffusivity is modeled by

$$\alpha = \frac{\alpha_\ell(\rho - \rho_{\text{v}}) + \alpha_{\text{v}}(\rho_\ell - \rho)}{\rho_\ell - \rho_{\text{v}}},$$

where ρ_ℓ (α_ℓ) and ρ_{v} (α_{v}) are the density (thermal diffusivity) of the liquid and vapor phase respectively.

At the discrete level, the spacial derivatives of Equation (8) are computed by means of the lattices discrete values and weights as describe by Li *et al.* (2018), regardless the type of boundary condition for T (Dirichlet or flux), no special treatment is needed at the boundaries since the *wet-node* approach is used for the LBE, as described in the next section. While the time derivatives are computed according to a second order Runge-Kutta method adapted from LeVeque (2007).

2.3 Hydrodynamical boundary conditions

2.3.1 Walls and inlet

The wet-node boundary conditions proposed by Zou and He (1997) are used to prescribe fluxes both at the wall and the inlet boundaries (see Fig. 1). For the left inlet this implies:

$$\rho^{\mathrm{b}} = \frac{1}{1-u_x^{\mathrm{b}}}\left(f_0 + f_2 + f_4 + 2\left(f_3 + f_6 + f_7\right) - \frac{\Delta t F_x^{\mathrm{b}}}{2}\right) , \tag{9}$$

$$f_1 = f_3 + \frac{2\rho^{\mathrm{b}} u_x^{\mathrm{b}}}{3} - \frac{\Delta t F_x^{\mathrm{b}}}{6} , \tag{10}$$

$$f_5 = f_7 - \frac{1}{2}\left(f_2 - f_4\right) + \frac{\rho^{\mathrm{b}} u_y^{\mathrm{b}}}{2} + \frac{\rho^{\mathrm{b}} u_x^{\mathrm{b}}}{6} - \frac{\Delta t F_x^{\mathrm{b}}}{6} - \frac{\Delta t F_y^{\mathrm{b}}}{4} , \tag{11}$$

$$f_8 = f_6 + \frac{1}{2}\left(f_2 - f_4\right) - \frac{\rho^{\mathrm{b}} u_y^{\mathrm{b}}}{2} + \frac{\rho^{\mathrm{b}} u_x^{\mathrm{b}}}{6} - \frac{\Delta t F_x^{\mathrm{b}}}{6} + \frac{\Delta t F_y^{\mathrm{b}}}{4} . \tag{12}$$

Where the superindex (^{b}) indicates boundary nodes. These formulas are adapted for each type of boundary according to:

***Inlet*:** The vertical velocities u_y^{b} are set to zero and

$$\left(u_x^{\mathrm{b}}\right)_j = -4\,U_{\max}(j-1)(j-N_y)/N_y^2, \qquad j = 1 \ldots N_y . \tag{13}$$

***Walls*:** The field $\mathbf{u}^b$ is neglected (no-slip condition), and the force vector $\mathbf{F}^{\mathrm{b}}$ is adapted to the fluid-solid interaction trough the tuning of the contact angle. To detail this, recall that at the bulk of the fluid the forces computed in Equation 6 are split as

$$F_\alpha^{\mathrm{SC}}(\mathbf{x}^{\mathrm{b}}, t) = -\psi(\mathbf{x}^{\mathrm{b}}, t)\left(G\sum_{i\in I^f} w_i \psi(\mathbf{x}^{\mathrm{b}} + \Delta t\,\mathbf{c}_i, t)\,c_{i\alpha} + G^{\mathrm{b}}\sum_{i\in I^s} w_i \psi(\mathbf{x}^{\mathrm{b}}, t)\,c_{i\alpha}\right) , \tag{14}$$

where I^f and I^s are the indices associated to fluid-fluid interactions and fluid-solid interactions respectively. This corresponds to the *modified ψ-based* model proposed by Li *et al.* (2014), where for this work we set $G^{\mathrm{b}} = -0.94$, a value found numerically to set a contact angle of $\pi/2$.

2.3.2 Outlet

The numerical schemes used to impose an outflow condition downstream are adapted from the ones studied by Lou *et al.* (2013), they require to employ ghost lattices as depicted in Figure 2. Two different methodologies were tested:

1. **Null Neumann Condition**

   This scheme aims to enforce a fully developed regime for the flow far away from the bulk of transient behavior sources (e.g., nucleation sites). For an arbitrary field $g(\mathbf{x}, t)$, its values $g^n_{N_x+1} \equiv g(\mathbf{x}^{\mathrm{b}} + \Delta t\,\mathbf{c}_1, t^n)$ (where $\mathbf{c}_1 = (1, 0)$) at the ghost lattices are computed according to

   $$g^n_{N_x+1} = g^n_{N_x} , \tag{15}$$

   which is a discretization of $\frac{\partial g}{\partial x} = 0$ at the outlet. In our implementation, this last rule was used to update all the fields $\mathbf{f}, \rho, \psi, \mathbf{u}, \mathbf{F}$ and T.

2. **Convective Condition**

   This conditions takes into considerations the possible transient variations near the outlet. For an arbitrary field $g(\mathbf{x}, t)$ the values at the neighbors of the outlet are updated by

   $$g^{n+1}_{N_x} = \frac{g^n_{N_x} - (u_x)^n_{N_x}\, g_{N_x-1}}{1 + (u_x)^n_{N_x}} , \tag{16a}$$

   $$g^{n+1}_{N_x+1} = \frac{g^n_{N_x+1} - (u_x)^n_{N_x+1}\, g_{N_x}}{1 + (u_x)^n_{N_x+1}} , \tag{16b}$$

   which correspond to discretizations of $\frac{\partial g}{\partial t} + u_x \frac{\partial g}{\partial x} = 0$ at the outlet for the discrete mesh parameters $\Delta t = 1$ and $\Delta x = 1$. The complex dependency between the macroscopic fields makes their computations at the outlet a non trivial matter. For instance, one may compute ψ according to (16a) or compute it from the values of T and ρ there. Thus, let us detail the chosen procedure based on what we observed to give stable results.

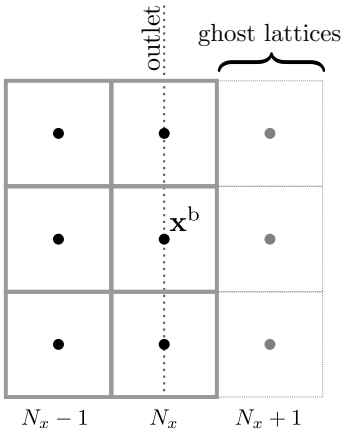

Figure 2. Ghost lattices placed at the outlet.

- After suitable initializations of all the fields at the boundary, $(u_x)_{N_x+1}^{n+1}$ is computed in time by means of (16b);
- The distributions field $\mathbf{f}(N_x, t)$ is computed from (16a);
- The values $\rho(N_x, t)$, $\psi(N_x, t)(N_x, t)$, $\mathbf{U}(N_x, t)$, $\mathbf{F}(N_x, t)$ and $T(N_x, t)$ are computed from their respective relations according to the LBE and the Energy Equation (8);
- $\psi(N_x + 1, t)$ is computed according to Equation (7);
- Finally, $\rho(N_x + 1, t)$, $\mathbf{U}(N_x + 1, t)$ and $T(N_x + 1, t)$ are computed by means of (16b).

2.4 Thermal boundary conditions

Excepting the nucleation site, the temperature field T was set to the saturation temperature T_s both at the inlet and the wall boundaries. At the outlet, T was computed by either the null Neumann condition or the convective condition described in the previous section. At the nucleation site the temperature was set to $T_b > T_c$, more details are given on Section 3.2.

2.5 Pseudocode outlook

For completeness, we give here the pseudocodes detailing the steps performed for the coupled computing of the LBE and the Runge-Kutta scheme.

2.5.1 Hydrodynamical calculations

Algorithm 1: Coupled LBE/Energy in time

Input: Initial fields ρ, $\mathbf{u}$ and T
Initialize distributions fields $\mathbf{f}$
for $n = 1 \ldots N - 1$ **do**
  $\mathbf{f}^{n+1}$ = **ComputeMRT**($\mathbf{f}^n$,ρ^n,ψ^n,$\mathbf{u}^n$,$\mathbf{F}^n$)
  T^{n+1} = **ComputeRK2**(T^n,ρ^n,$\mathbf{u}^n$)
  [ρ^{n+1},ψ^{n+1},$\mathbf{u}^{n+1}$,$\mathbf{F}^{n+1}$] = **ComputeMacroscopics**($\mathbf{f}^{n+1}$,T^{n+1},$\mathbf{u}^n$)
end

The function **ComputeMRT** performs the computations related to the LBE and returns the new distributions field, while **ComputeRK2** returns the new temperature field by means of a second order Runge Kutta method and **ComputeMacroscopics** returns the new values of the macroscopic fields.

2.5.2 Thermal calculations

Algorithm 2: ComputeRK2

Input: T^n,ρ^n,$\mathbf{u}^n$
Output: T^{n+1}

| *Set boundary conditions for temperature*
$T^n = \textbf{SetBndryCnds}(T^n)$
| *Compute the Runge-Kutta terms*
$h_1 = \textbf{ComputeH}(T^n, \rho^n, \mathbf{u}^n)$
$h_2 = \textbf{ComputeH}(T^n + h_1, \rho^n, \mathbf{u}^n)$
| *Compute the updated temperature*
$T^{n+1} = T^n + \frac{1}{2}(h_1 + h_2)$

The function **SetBndryCnds** set the values of T at the boundary, which, at the ghost cells, depend on the strategy chosen at the outlet. The function **ComputeH** computes the Runge-Kutta terms (which are approximations of the righ-hand-side of the evolution equation for T). Observe that h_1 and h_2 also depend on whether one uses the Null Neumann condition or the convective condition, which is encoded in **ComputeH**.

3. NUMERICAL RESULTS

In this section, we apply the previously discussed algorithms to model channel flows. First, we evaluate the outflow boundary conditions in the case of a vapor bubble surrounded by liquid flowing in a channel without heat transfer. After this, the lattice Boltzmann method is applied to simulate the nucleation of a bubble in a channel flow and study the impact of the boundary conditions and contact angle. The results and numerical parameters are presented in lattice units, the non-dimensional numbers needed to convert the results to other compatible settings are provided.

3.1 Hydrodynamic tests

The hydrodynamic test performed in this subsection consist in a vapor bubble surrounded by liquid flowing inside a channel. The channel dimensions are $(L_x, L_y) = (200, 50)$ and the flow is initialized at saturated conditions at $T_r = 0.86$ where the saturated densities are given by $\rho_v = 0.38$ and $\rho_l = 6.50$. The bubble is initialized with a circular geometry of radius $r = 20$ in the position $(L_{bx}, L_{by}) = (50, 25)$. A parabolic velocity profile uniform at the x-direction is set at the initial time. The viscous relaxation time is set as $\tau_v = 0.8$ which results in a kinematic viscosity of $\nu = 0.1$. The Reynolds number and Weber number used in this test are $Re = 80$ and $We = 97$. The temperature field is maintained constant along the simulation.

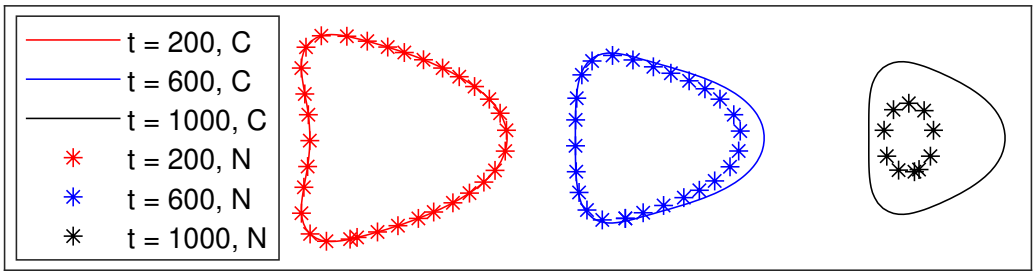

Figure 3. Bubble flow with $Re = 80$, $We = 97$ without the addition of the force $F_x = \rho 8 \nu_l U_{max}/L_y^2$. The convective boundary condition is represented by "C" and the Neumann boundary condition by "N".

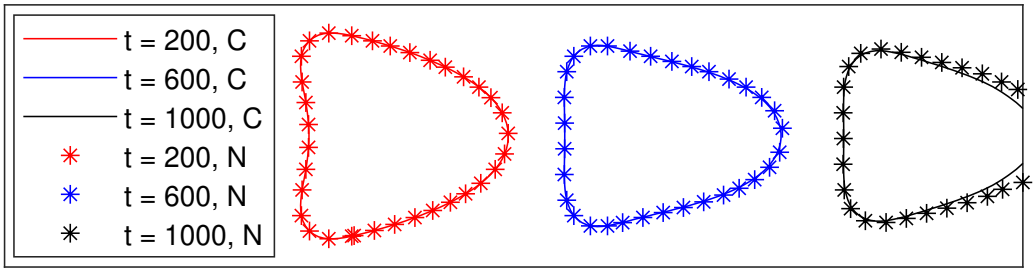

Figure 4. Bubble flow with $Re = 80$, $We = 97$ with the addition of the force $F_x = \rho 8 \nu_l U_{max}/L_y^2$. The convective boundary condition is represented by "C" and the Neumann boundary condition by "N".

The bubble position at different times are shown in Figure 3 both for the convective and Neumann boundary conditions at the outflow. The time is given in lattice units but it can be converted to non-dimensional time by $t^* = tU_{max}/L_y$, where $U_{max} = \nu_l Re/L_y$. In both simulations it was observed the reduction of the bubble size along the flow direction. In the case of the Neumann boundary condition the bubble disappeared completely before reaching the outflow boundary. It was considered that this effect could be caused by an initialization issue. Since the LBM is a pseudo-compressible method Krüger *et al.* (2017), there is a pressure-density dependency. As the density initialization was not accounting for the pressure drop along the channel, the flow have a tendency to be slowed due to friction and by consequence the bubble is compressed. A simple procedure to avoid this issue is to add a force in the x-direction that accounts for the pressure drop due to friction effects. In this way we added the force $F_x = \rho 8\nu_l U_{max}/L_y^2$ which comes from the analytical solution of a Poiseuille flow between two infinite parallel plates. The bubble flow results obtained from the addition of that force are shown in Figure 4. In this case, the bubble condensation issue was avoided and the results for both boundary conditions were very similar.

3.2 Thermal flow tests

In this subsection, we evaluate how each boundary condition impacts on the nucleation of a bubble in the channel flow. We simulate the same channel geometry of the previous subsection. A higher temperature $T_b = 1.25T_c$ is set at the three nodes in the middle of the bottom wall. In this test, a bubble is still initialized because it was observed that this initial bubble helps the nucleation in the heated surface. A procedure to induce bubble nucleation in a physically consistent manner from a domain completely filled with liquid will be investigated in future works. In this work the focus is to study differences in the flow due to the boundary conditions. The Reynolds number was reduced to $Re = 50$ in order to favor the bubble nucleation. The Weber number also changes (due to the new flow velocity) to $We \approx 38$. The contact angle used in the next simulations is $\theta = 90^o$. The Péclet and Jacob numbers were set as $Pe = 83$ and $Ja = 0.42$. The density fields at different times for the convective boundary are shown in Figure 5. One can observe that a small vapor nucleus is formed above the heated lattices but this nucleus did not departed from the surface.

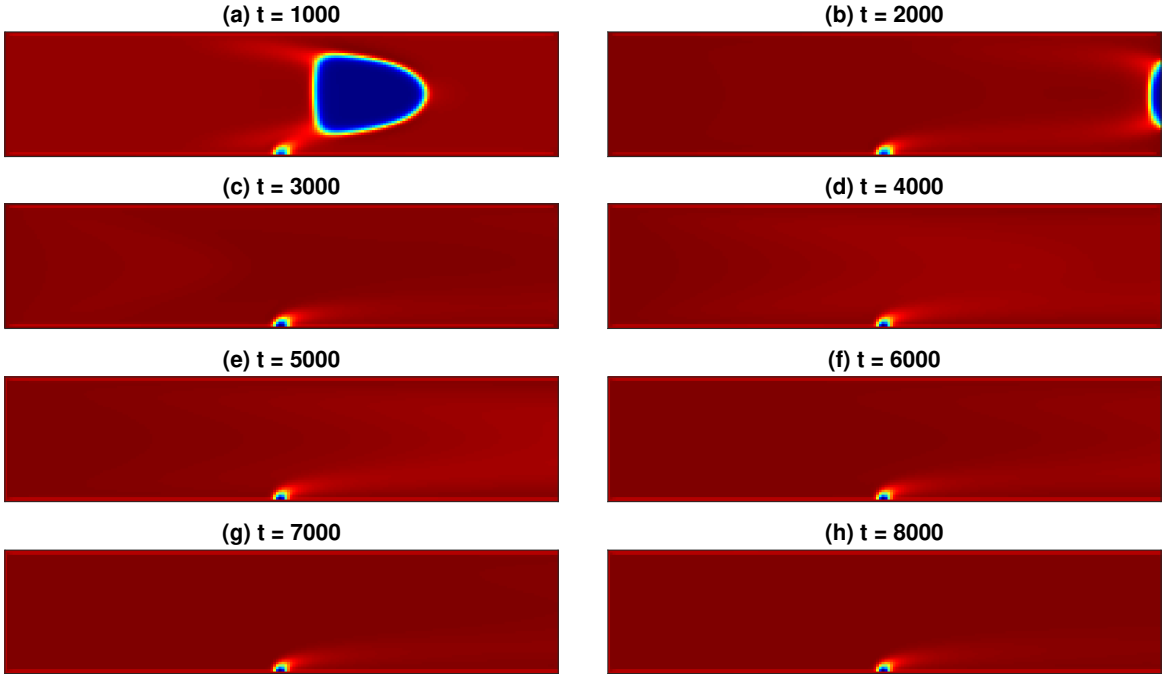

Figure 5. Boiling flow with Re=50 and contact angle $\theta = 90^o$ using the convective boundary condition.

It was noticed an issue with respect to the convective boundary condition. Since the velocity at the walls are zero, the distribution functions at the corners of the outlet boundary do not change in time (see Equation (16a)). To test if this fact can significantly impact the flow field, we considered in Equations (16a) and (16b) that the velocities at the corners are equal to the velocities of the neighbor nodes as $u(1, N_x, t) = u(2, N_x, t)$ and $u(N_y, N_x, t) = u(N_y - 1, N_x, t)$. The results of this modification are shown in Figure 6. This time, differently from the previous results, the vapor nucleus grows to form a vapor film that covers the bottom surface.

Results considering the Neumann boundary condition are shown in Figure 7. Until the simulation time $t = 4000$ results are similar to the ones obtained with the convective boundary condition. But after this time, the respective simulations differ as the liquid film now detaches from the initial vapor nucleus and a new vapor film starts to grow.

In the next simulations we change the surface wetting condition to became more hydrophilic by changing G^b to

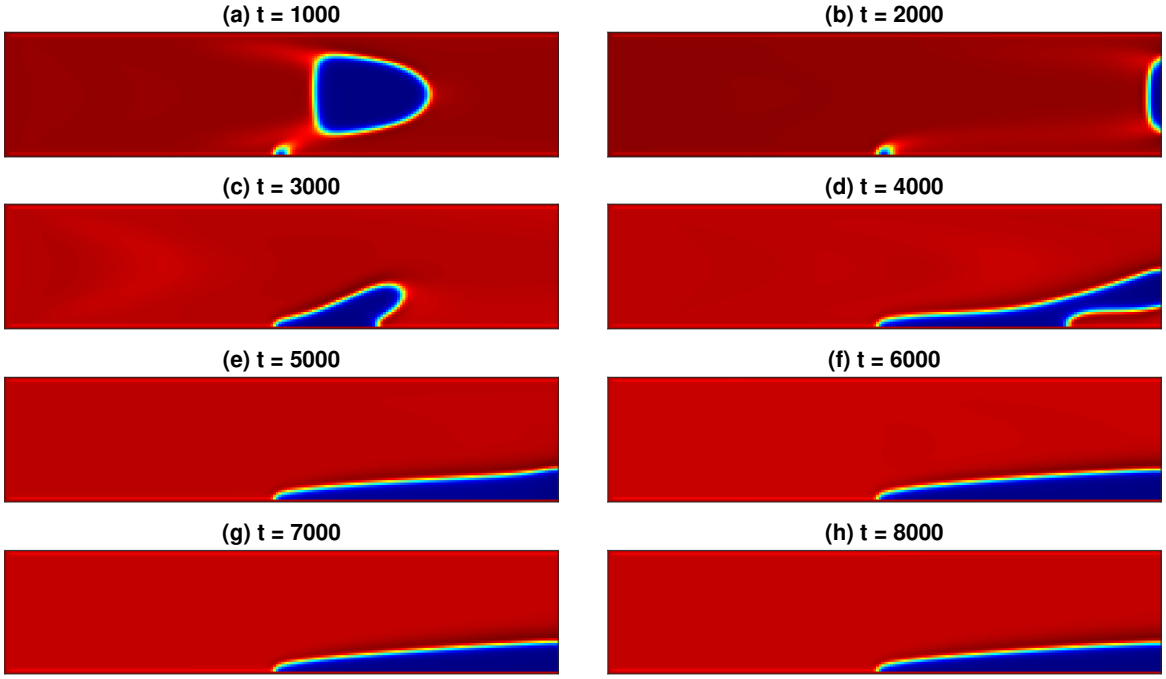

Figure 6. Boiling flow with Re=50 and contact angle $\theta = 90^o$ using the convective boundary condition with modified corners.

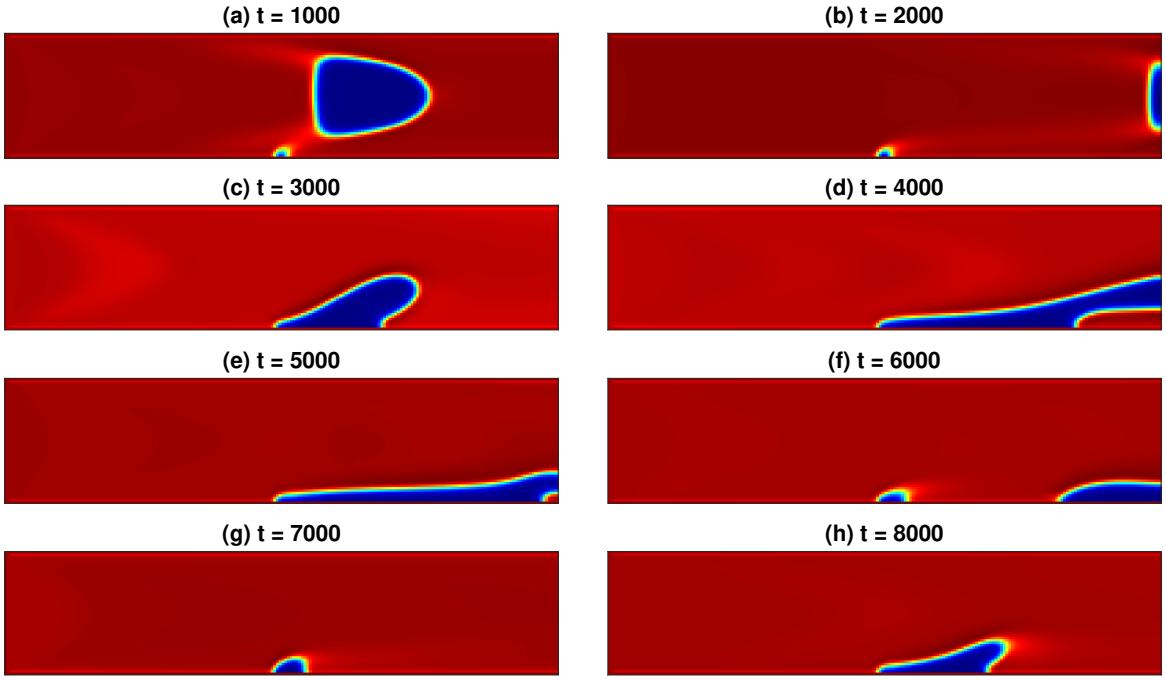

Figure 7. Boiling flow with Re=50 and contact angle $\theta = 90^o$ using the Neumann boundary condition.

-1.5 in Equation (14). Simulation results considering the convective and Neumann boundary conditions are shown in Figures (8) and (9), respectively. Differently from the previous results, where a film of liquid was induced from the nucleation site, the formation of bubbles that detach periodically from the heated surface can be observed. It seems also, that the bubble growth is triggered by the previous bubble leaving the domain. Observe that this is in accordance with the previous observation of the need for an initial bubble in order for the nucleation to take place. In the case of the Neumann boundary condition, only one bubble cycle was observed.

4. CONCLUSIONS AND FUTURE WORK

This work presents first results on bubble nucleation in channels induced by heat transfer along the LBM. Although there exist several numerical works assessing the introduction of physical two-phase features like contact angle, surface

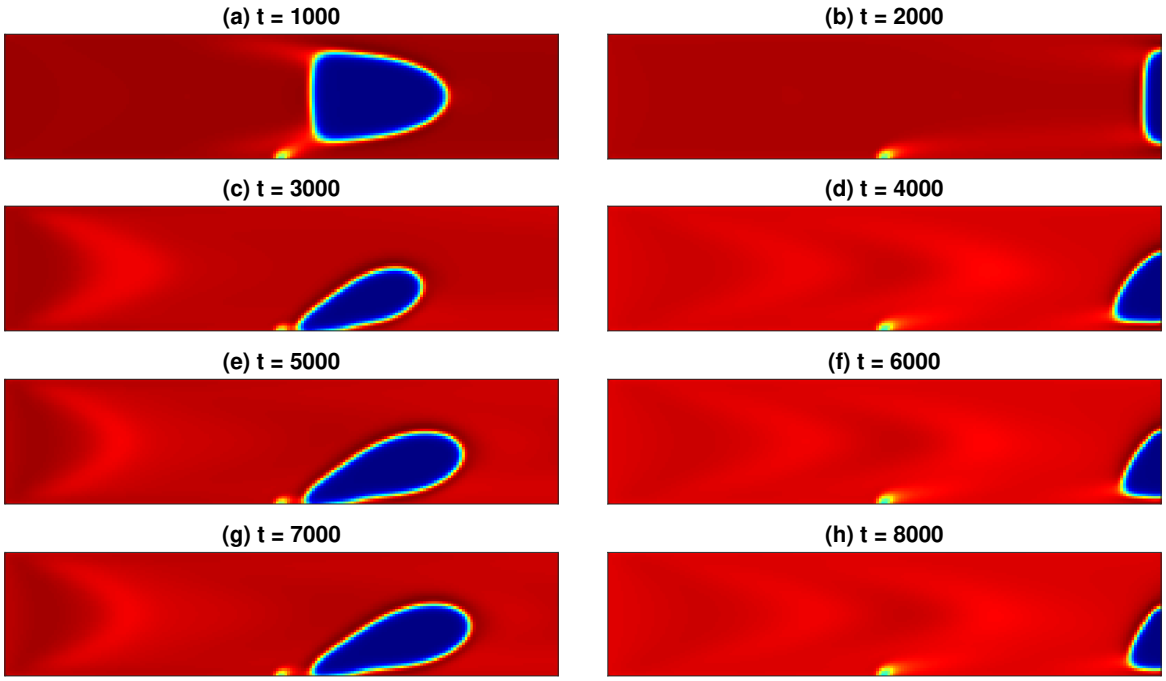

Figure 8. Boiling flow with Re=50 and hydrophilic wetting condition in the solid surface using the convective boundary condition.

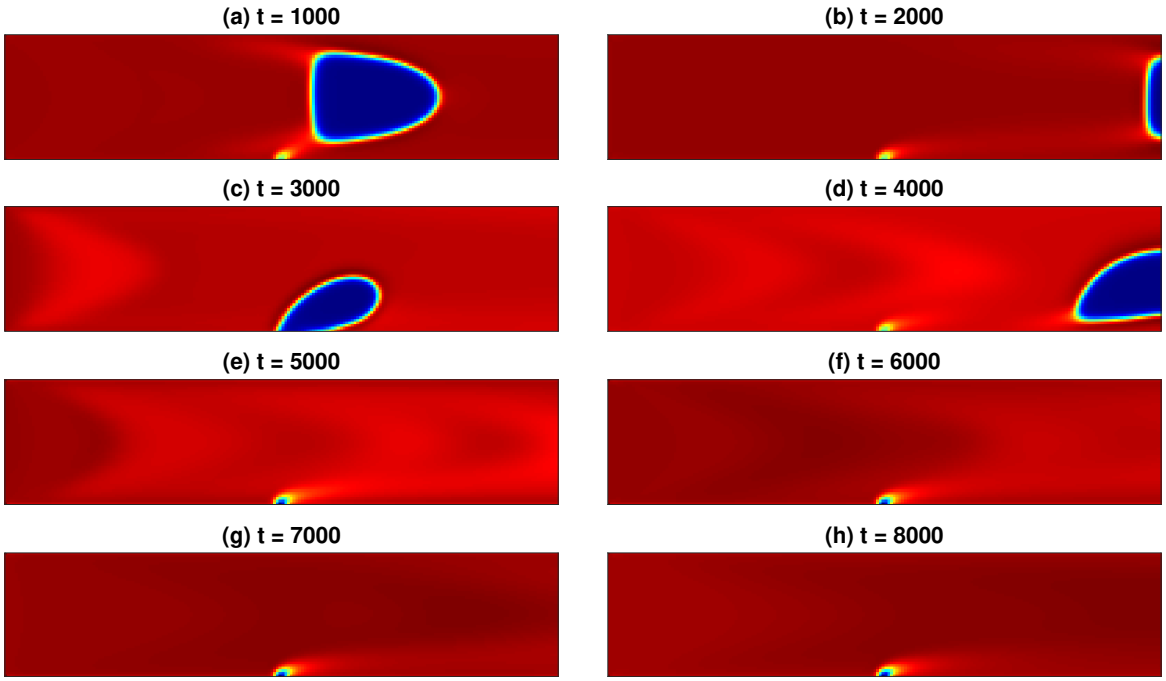

Figure 9. Boiling flow with Re=50 and hydrophilic wetting condition in the solid surface using the Neumann boundary condition.

tension and heat transfer in a separately fashion, there is a lack of literature where all these features are included at once. Moreover, fluid flow in channels require to address suitable discrete treatment of the meso and macroscopic fields at the outlets. Different outflow models are available in the literature, but their impact on the different macroscopic field involved in these simulations is unclear.

We have performed simulations imposing a velocity profile at the inlet of the channel and used two different discrete outflow boundary conditions. Bubble nucleation was observed to be induced only when the initial condition for the density field included an already formed bubble of vapor. Moreover, the convective outflow boundary condition was found to induce bubble nucleation by a larger amount of time (many bubble cycles) when compared to the results along the Neumann condition. Also, as expected, the bubble's depart takes place sooner for larger contact angles, as this implies the surface of the channel to be more hydrophilic, inducing the bubble to extend beyond the temperature pertubation site.

Future work will include more detailed results to analyse the dependence of nucleation and heat transfer efficiency on the initial conditions and the outflow implementation. Also, further research will include lower reduced temperatures, comparisons of bubble formation flow patterns with experimental results, and three-dimensional settings. $R = 1$

5. ACKNOWLEDGEMENTS

The authors gratefully acknowledge the financial support received from the São Paulo Research Foundation FAPESP grants 2016/09509-1, 2018/09041-5 and 2020/12919-2, and from the National Council for Scientific and Technological Development (CNPq), process 431782/2018-0.

6. REFERENCES

Chen, S. and Doolen, G.D., 1998. "LATTICE BOLTZMANN METHOD FOR FLUID FLOWS". *Annual Review of Fluid Mechanics*, Vol. 30, No. 1, pp. 329–364.

Genk, M., 2012. "Immersion cooling nucleate boiling of high power computer chips". *Energy Conversion and Management*, Vol. 53, No. 1, pp. 205–218.

Guzella, M., Czelusniak, L., Mapelli, V., Fariñas, P., Ribatski, G. and Cabezas-Gómez, L., 2020. "Simulation of boiling heat transfer at different reduced temperatures with an improved pseudopotential lattice boltzmann method". *Symmetry*, Vol. 12, No. 8, p. 1358.

Hu, A., Li, L., Uddin, R. and Liu, D., 2016. "Contact angle adjustment in equation-of-state-based pseudopotential model". *Physical Review E*, Vol. 93, No. 5.

Jafari, R. and Okutucu-Özyurt, T., 2016. "Numerical simulation of flow boiling from an artificial cavity in a microchannel". *International Journal of Heat and Mass Transfer*, Vol. 97, pp. 270–278.

Krüger, T., Kusumaatmaja, H., Kuzmin, A., Shardt, O., Silva, G. and Viggen, E., 2017. *The Lattice Boltzmann Method*. Springer International Publishing.

LeVeque, R., 2007. *Finite Difference Methods for Ordinary and Partial Differential Equations*. Society for Industrial and Applied Mathematics.

Li, Q. and Luo, K., 2013. "Achieving tunable surface tension in the pseudopotential lattice boltzmann modeling of multiphase flows". *Physical Review E*, Vol. 88, No. 5.

Li, Q., Luo, K., Kang, Q. and Chen, Q., 2014. "Contact angles in the pseudopotential lattice boltzmann modeling of wetting". *Physical Review E*, Vol. 90, No. 5.

Li, Q., Yu, Y. and Wen, Z.X., 2020. "How does boiling occur in lattice boltzmann simulations?" *Physics of Fluids*, Vol. 32, No. 9, p. 093306.

Li, Q., Yu, Y., Zhou, P. and Yan, H., 2018. "Enhancement of boiling heat transfer using hydrophilic-hydrophobic mixed surfaces: A lattice boltzmann study". *Applied Thermal Engineering*, Vol. 132, pp. 490–499.

Lou, Q., Guo, Z. and Shi, B., 2013. "Evaluation of outflow boundary conditions for two-phase lattice boltzmann equation". *Physical Review E*, Vol. 87, No. 6.

Park, S., Kim, J. and Bang, I., 2016. "Experimental study on a novel liquid metal fin concept preventing boiling critical heat flux for advanced nuclear power reactors". *Applied Thermal Engineering*, Vol. 98, pp. 743–755.

Pulvirenti, B., Matalone, A. and Barucca, U., 2010. "Boiling heat transfer in narrow channels with offset strip fins: Application to electronic chipsets cooling". *Applied Thermal Engineering*, Vol. 30, No. 14-15, pp. 2138–2145.

Sohankar, A., Norberg, C. and Davidson, L., 1998. "Low-reynolds-number flow around a square cylinder at incidence: study of blockage, onset of vortex shedding and outlet boundary condition". *International Journal for Numerical Methods in Fluids*, Vol. 26, No. 1, pp. 39–56.

Sukop, M. and Thorne, D., 2006. *Lattice Boltzmann Modeling*. Springer Berlin Heidelberg.

Zhang, R. and Chen, H., 2003. "Lattice boltzmann method for simulations of liquid-vapor thermal flows". *Phys. Rev. E*, Vol. 67, p. 066711.

Zou, Q. and He, X., 1997. "On pressure and velocity boundary conditions for the lattice boltzmann BGK model". *Physics of Fluids*, Vol. 9, No. 6, pp. 1591–1598.

7. RESPONSIBILITY NOTICE

The authors are solely responsible for the printed material included in this paper.